Immunopathogenesis of Graft Fibrosis Following Liver Transplantation: A Spatial Profiling Approach Using Imaging Mass Cytometry

Joseph Katz and Dr. Mamatha Bhat

UNIVERSITY OF TORONTO

DEFY GRAVITY

Background and Introduction

Hepatic Stellate Cell

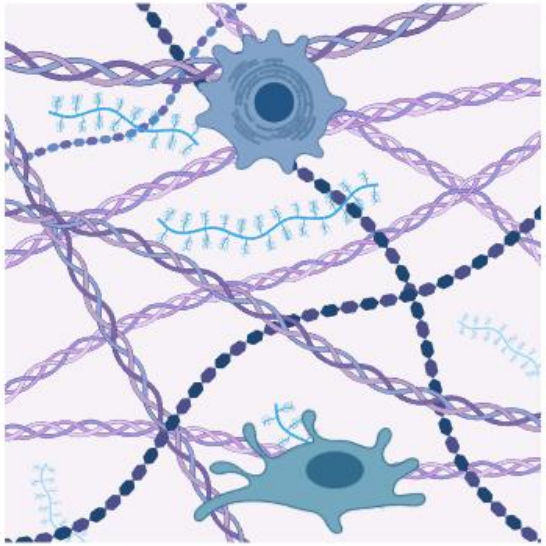

Kupffer Cell

- Liver Fibrosis in allograft health post-transplant.
  - CD163+ Kupffer cells driving Extracellular Matrix deposition, hepatic stellate cells producing collagen, T cell inflammatory signalling, TGF-β signalling.
- Imaging Mass Cytometry (IMC): Spatial proteomics using metal-conjugated antibodies, CyTOF mass spectrometry.
  - Antibodies specific for immune markers (ie. CD45, CD4, CD8, HLA-DR, FOXP3, etc.) to map out immune cells within the fibrotic liver
- Prior studies show basic molecular drivers and cell types contributing to fibrosis, but limited knowledge on spatial organization of immune cells, heterogenous immune states, shifts in global immune composition.

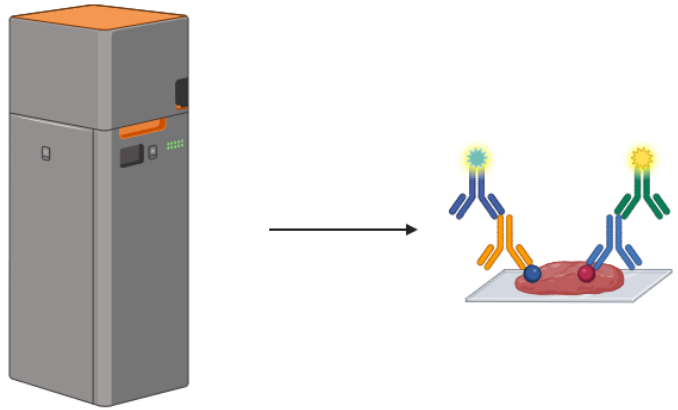

UNIVERSITY OF TORONTO

Project Objective

Objective: Determine whether fibrotic progression is associated with coordinated changes in immune composition and marker expression, and to identify the dominant factors underlying these changes.

Methods – Preprocessing, Segmentation, Extraction, and Clustering

1. Data Acquisition and Preprocessing: 40 samples, 2 regions of interest (ROIs) 750 µm × 750 µm. Sample 1 pre-fibrosis and Sample 2 with stage 2 fibrosis.
   - Normalized from 0 to 1 then arcsinh(x/5) – compress high signals and expand low signals
   - 57 markers – 25 biological, 8 calibration, 2 DNA, 22 isotope background channels
   - 2691 pre-fibrotic and 1754 fibrotic cells identified
2. Cell Segmentation and Cell Filtering: 2-channel .tif images using Mesmer (membrane + nuclear composite). Boundaries created.
3. Dimensionality Reduction and Clustering: Principal Component Analysis then k-means clustering. UMAP and t-SNE.

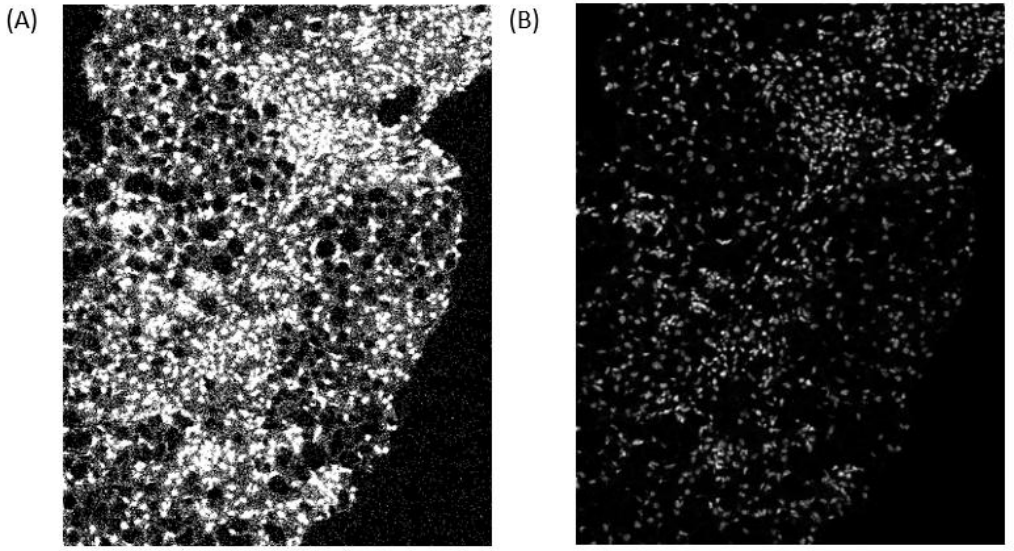

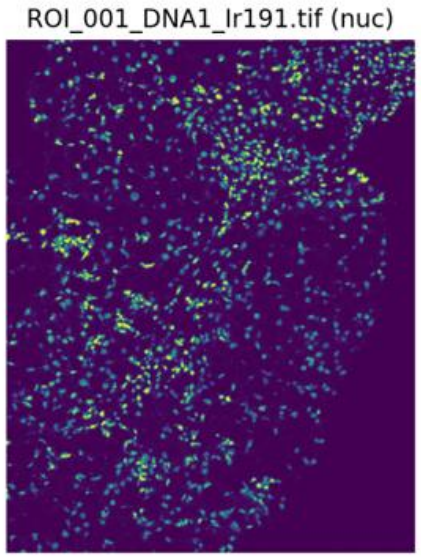

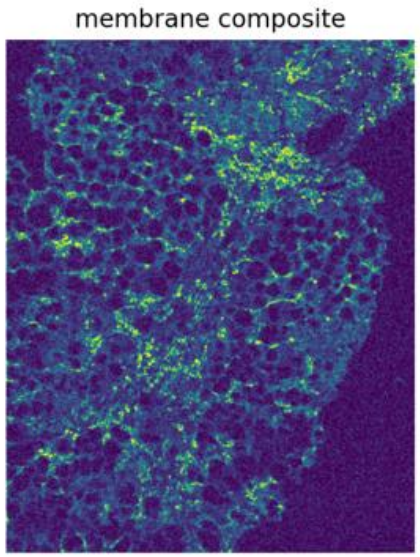

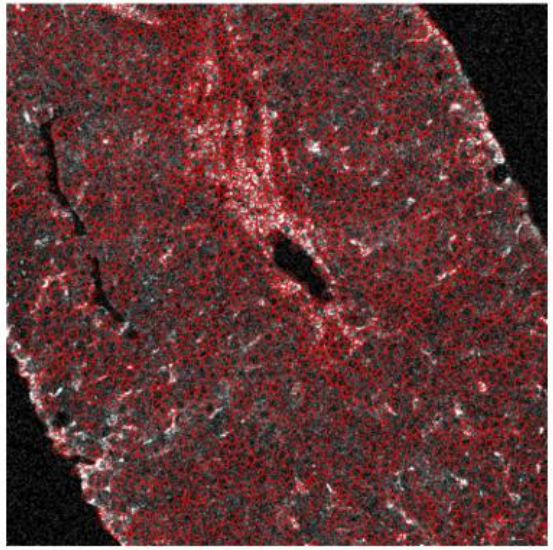

UNIVERSITY OF TORONTO

Global Cell Composition Changes

- Principal component analysis + k-means clustering → decision-tree
- 8 meta-clusters created by marker intensity gating
- Composition was similar between conditions
  - Increases in B cells (9.0% to 10.1%), CD8 T cells (2.5% to 5.1%), and NK cells (5.7% to 6.7%)
  - Decreases in Tregs (3.4% to 2.4%) and other immune cells (60.4% to 55.6%)
  - CD4 T cells and Myeloid populations remained stable.

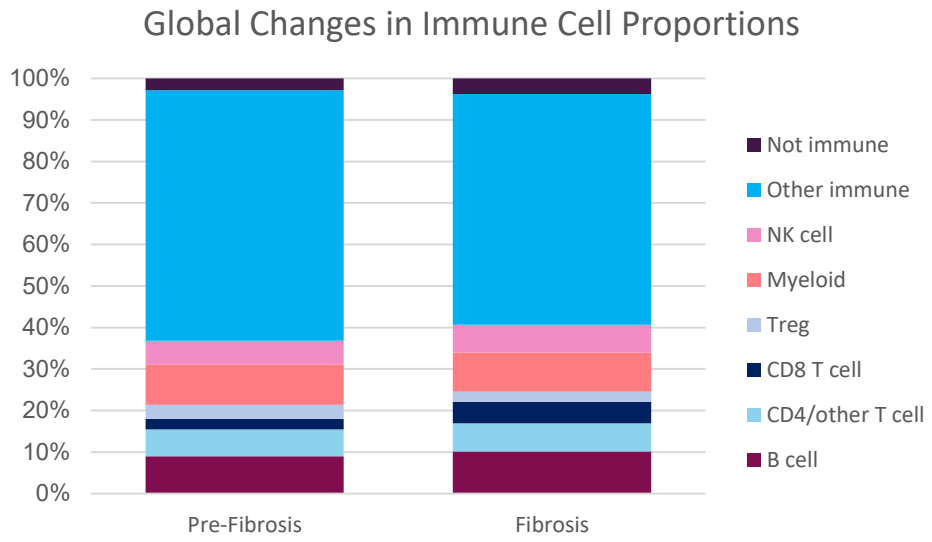

Row Labels	Pre-Fibrosis	Fibrosis
B cell	0.090242	0.10176
CD4/other T cell	0.064285	0.067769
CD8 T cell	0.025279	0.051165
Treg	0.034143	0.024982
Myeloid	0.097168	0.094083
NK cell	0.056874	0.067009
Other immune	0.603687	0.555941
Not immune	0.028322	0.03729

UNIVERSITY OF TORONTO

Dimensionality Reduction – UMAP/t-SNE

- Principal component analysis + k-means clustering → decision-tree for meta-cluster creation
- UMAP – revealed continuous distributions, partial clustering by cell type.
  - Immune cell populations in the periphery and non-immune cells in center
  - Pre-fibrosis: more diffuse distribution, less distinct clusters. More B cell and Treg clustering.
  - Fibrosis: increased regional organization, myeloid cluster formation, adjacent to CD8 T-cell cluster. Less B cell and Treg clustering.

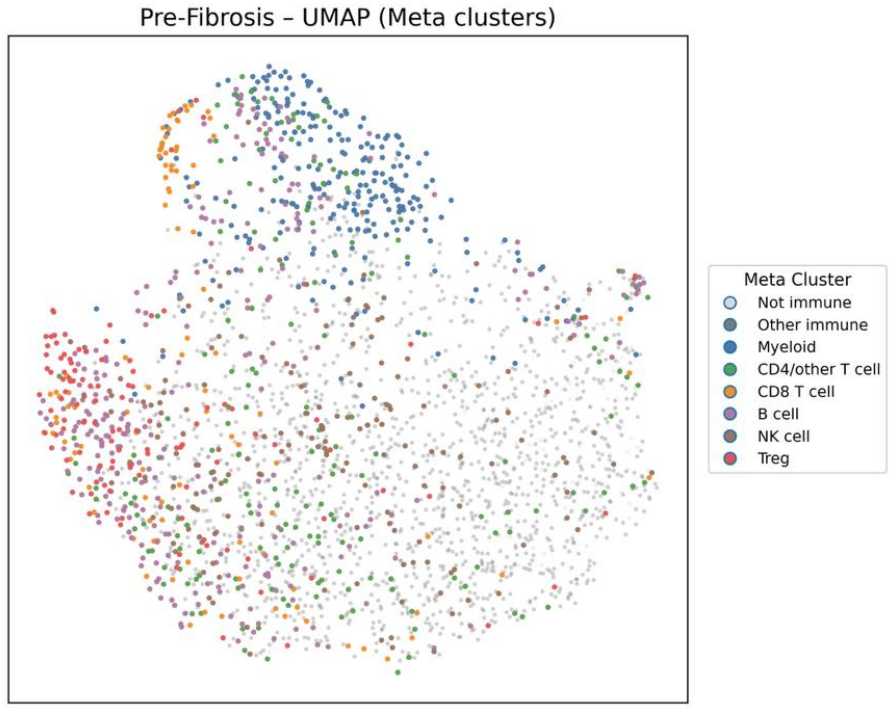

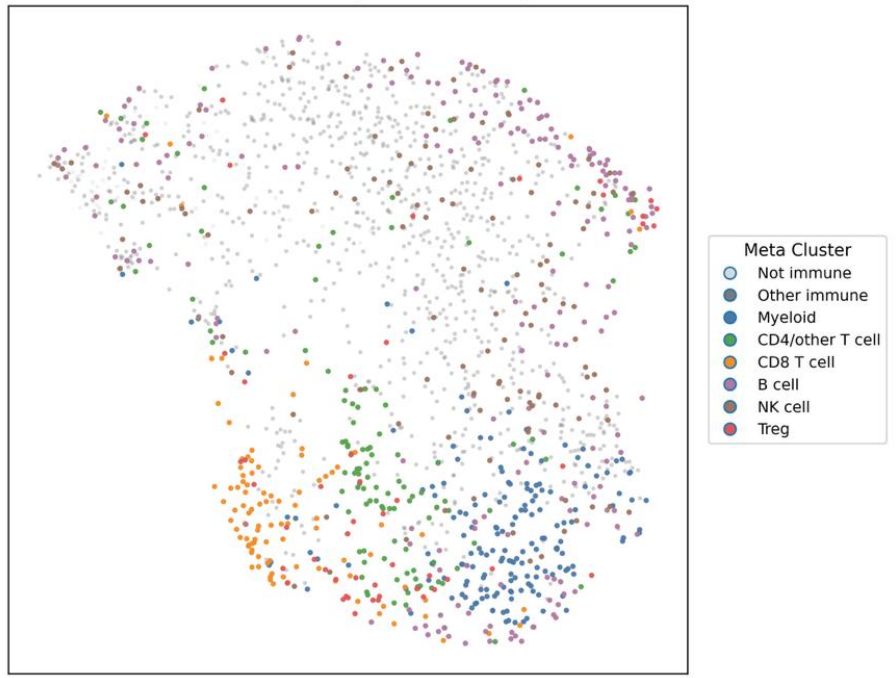

UNIVERSITY OF TORONTO

Dimensionality Reduction – UMAP/t-SNE

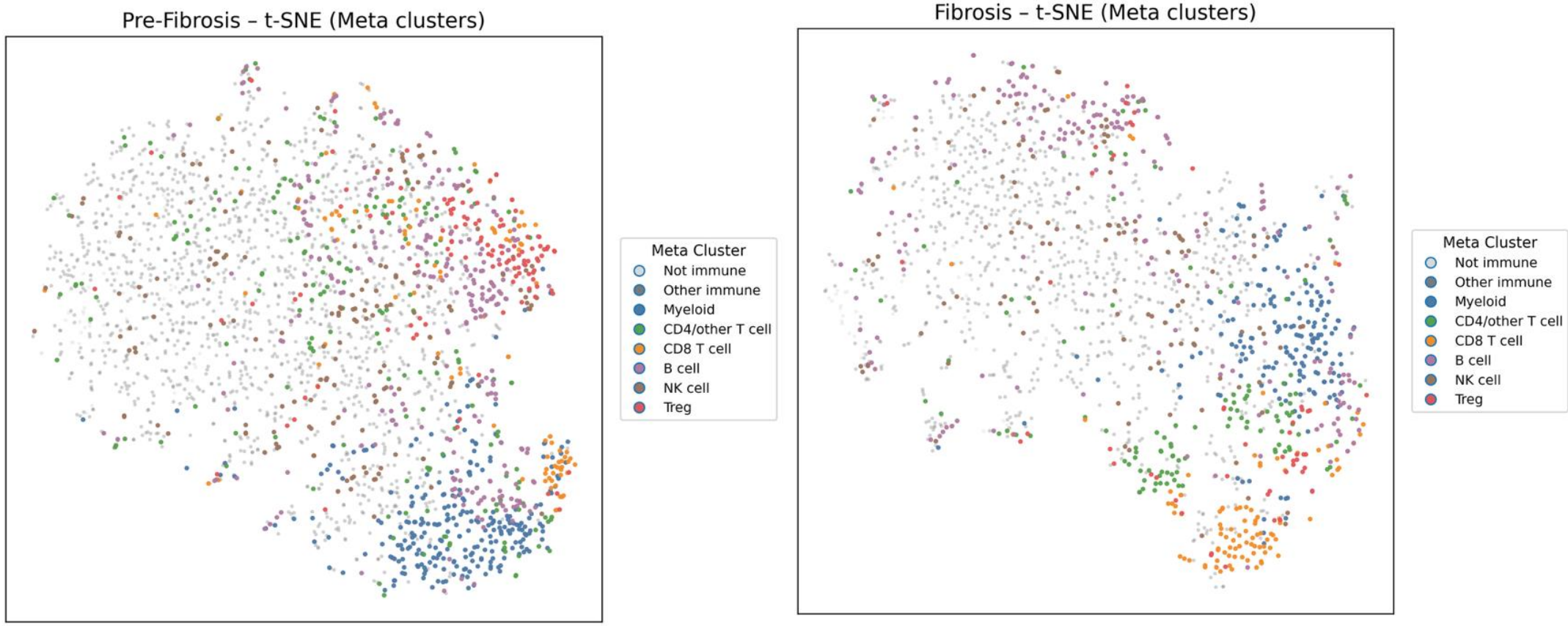

Principal Component Analysis – Variance Explained and PC1/PC2

- PC1 (12.0%): positive TIM3, CD16, HLA-DR, CD4 – activation axis
- PC2 (7.3%): positive CD279, FOXP3, CD20 and negative CD16, CD45, CD68 – adaptive vs. innate axis

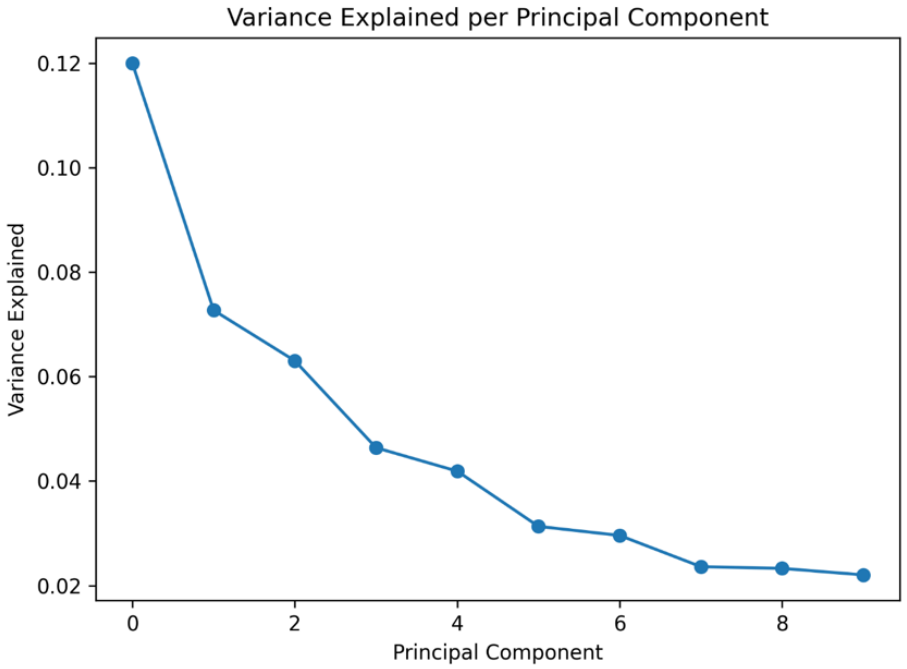

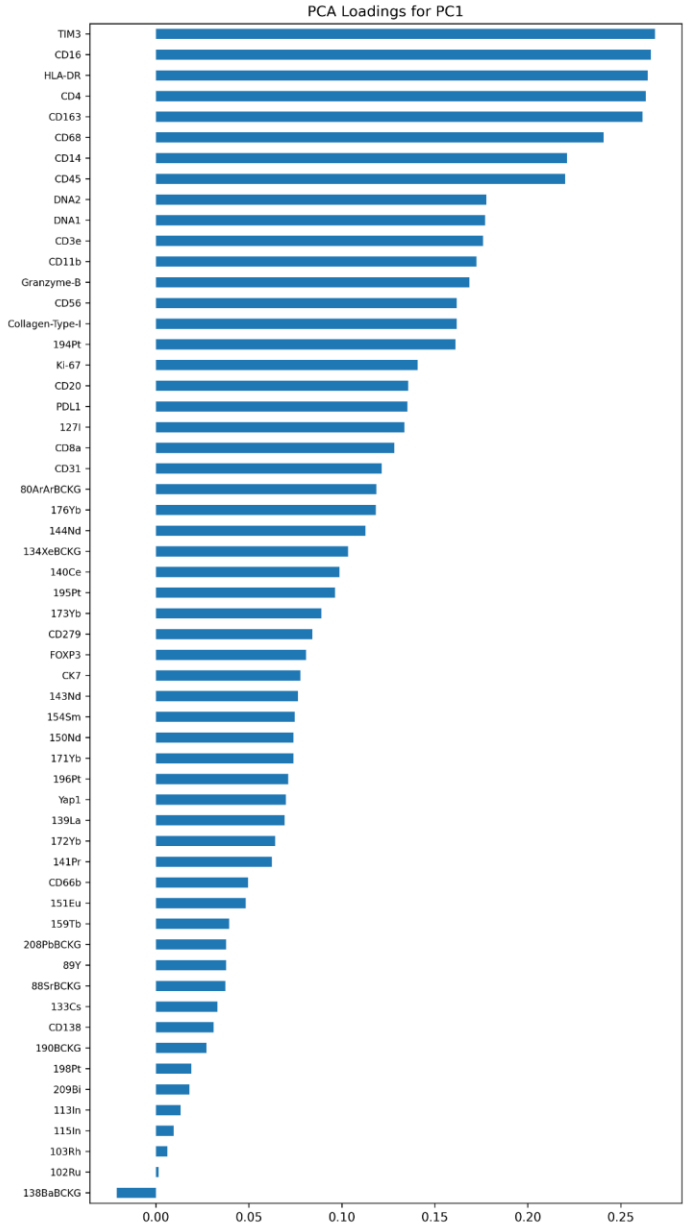

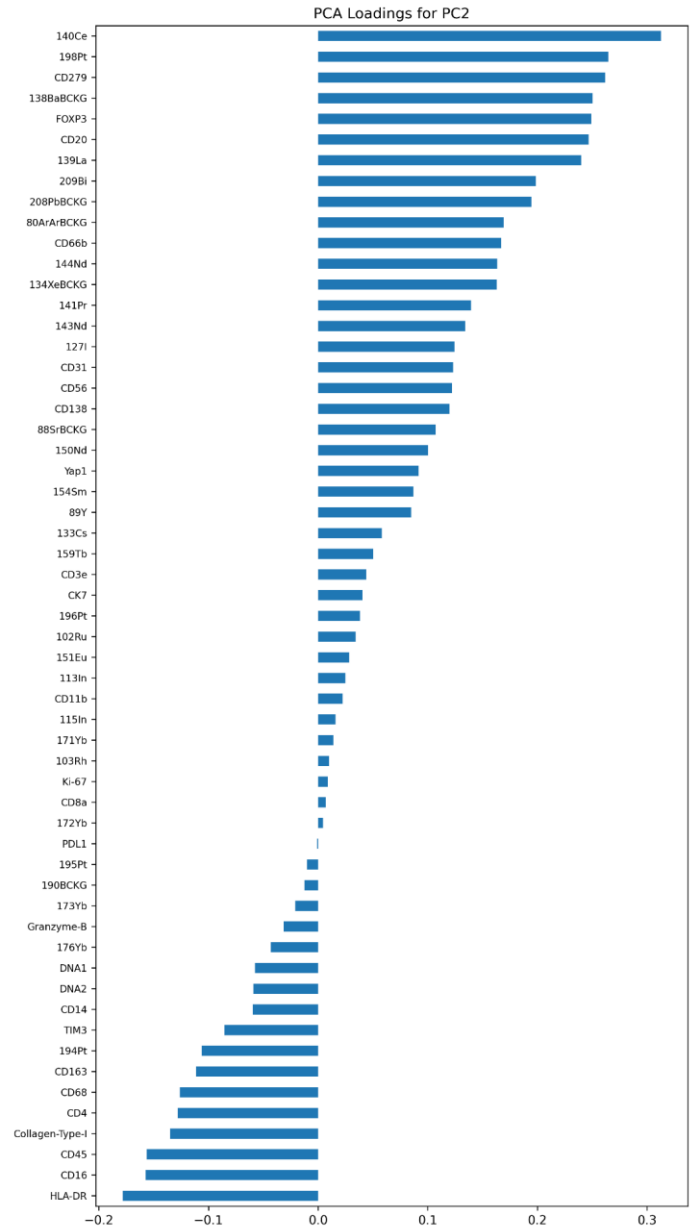

Principal Component Analysis - Distributions

PC1-PC2 space: substantial overlap between samples along PC1, greater separation along PC2

PC1 axis: similar means (nonfibrotic: -0.049, fibrotic: 0.075) and no significant difference (Welch p = 0.146; Mann-Whitney p = 0.606; Cohen's d = -0.047)

PC2 axis: separation of means (nonfibrotic: 0.253, fibrotic: -0.388) and significant difference/effect (Welch p = 6.70×10^{-24}; Mann-Whitney p = 2.46×10^{-37}; Cohen's d = 0.319)

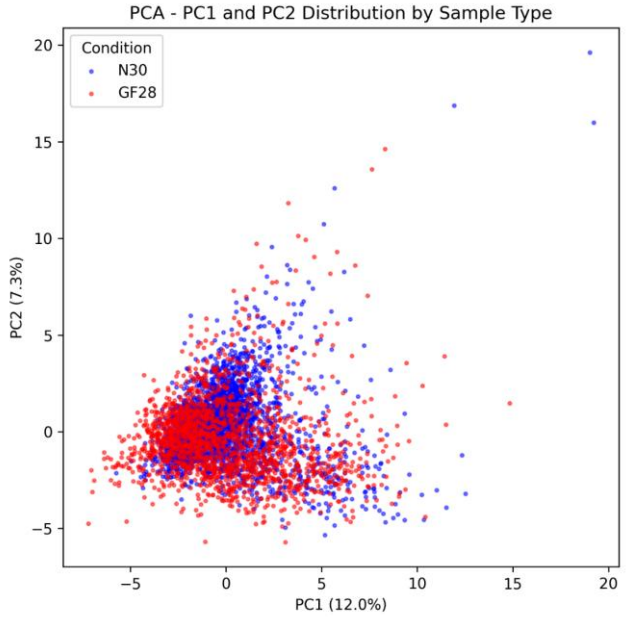

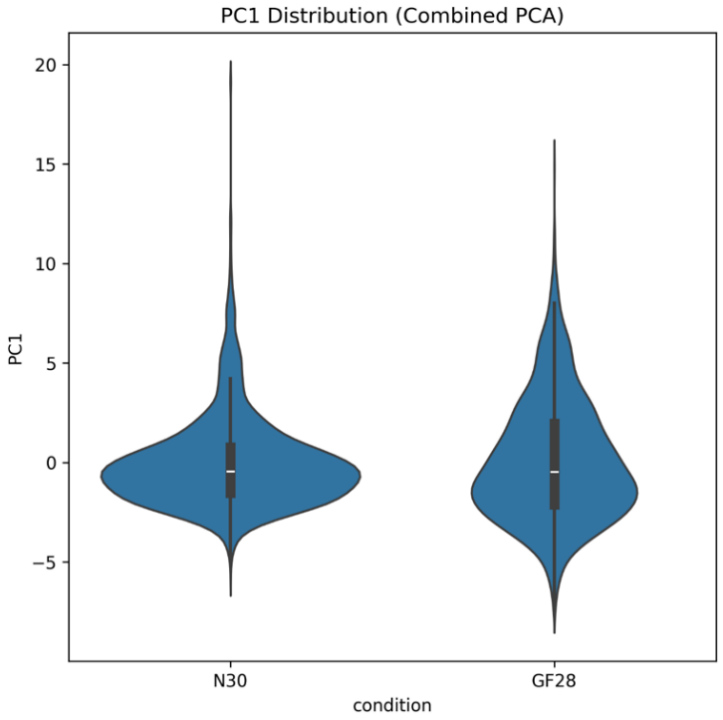

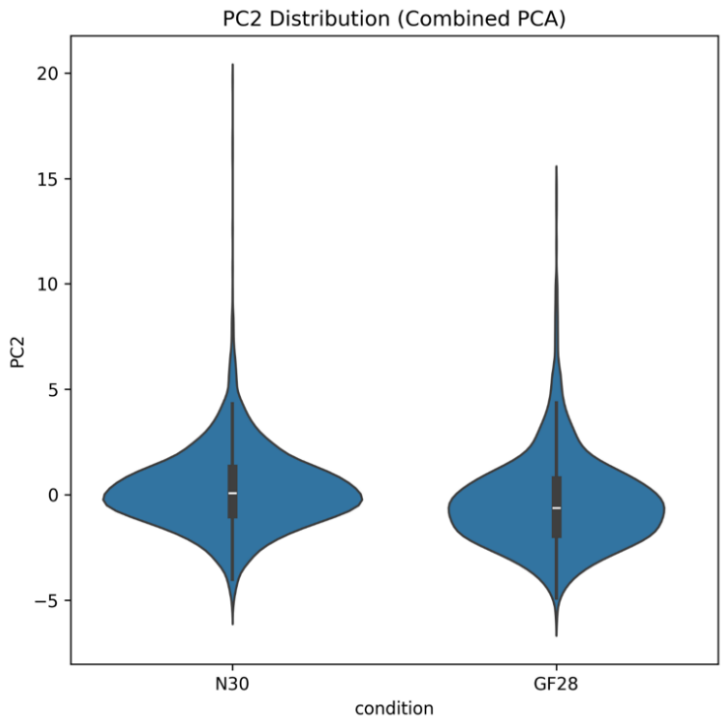

Metric	Value
N30_mean_PC1	-0.04873
GF28_mean_PC1	0.074759
N30_median_PC1	-0.4495
GF28_median_PC1	-0.4649
Welch_t_stat_PC1	-1.45263
Welch_t_pvalue_PC1	0.14643
MannWhitney_U_stat_PC1	2381575
MannWhitney_pvalue_PC1	0.606033
Cohens_d_PC1	-0.04723
N30_mean_PC2	0.253184
GF28_mean_PC2	-0.38844
N30_median_PC2	0.073655
GF28_median_PC2	-0.61695
Welch_t_stat_PC2	10.15645
Welch_t_pvalue_PC2	6.70E-24
MannWhitney_U_stat_PC2	2893956
MannWhitney_pvalue_PC2	2.46E-37
Cohens_d_PC2	0.318959

Conclusions, Limitations, and Next Steps

- Success of using IMC to capture microenvironment changes – not simply compositional change but reorganization in activation states and heterogeneity in subpopulations.
- UMAP/t-SNE suggest change in immune polarization/states. Myeloid and CD8 T cell coordination and single-state activation in fibrosis (aligns with traditional understanding).
- Overall PCA suggests similar amounts of immune activation but a leniency towards innate activity and macrophage activity in the fibrotic state.
- **Limitations:** Pseudo-replication in PCA analysis inflating p-values, 1 patient's single ROI, k-means k = 12 as standard value, decision-tree classification
- Next steps/future directions: all 40 patients with multiple ROIs, patient-level/structural-level analysis using Ilastik or CellProfiler, integrate clinical variables into multi-modal model.

References

1. Kisseleva, T., and D. A. Brenner. 2021. Mechanisms of fibrogenesis. *Nat. Rev. Gastroenterol. Hepatol.* 18: 151–166.

2. Ramachandran, P., A. Dobie, J. R. Wilson-Kanamori, E. Dora, B. E. Henderson, et al. 2019. Resolving the fibrotic niche of human liver cirrhosis at single-cell level. *Nature* 575: 512–518.

3. Giesen, C., H. A. Wang, D. Schapiro, N. Zivanovic, A. Jacobs, et al. 2014. Highly multiplexed imaging of tumor tissues with subcellular resolution by mass cytometry. *Nat. Methods* 11: 417–422.

4. Schapiro, D., H. W. Jackson, S. Raghuraman, J. R. Fischer, V. Zanotelli, et al. 2017. histoCAT: analysis of cell phenotypes and interactions in multiplex image cytometry data. *Nat. Methods* 14: 873–876.

5. Windhager, J., D. Bodenmiller, and B. Bodenmiller. 2019. An end-to-end workflow for multiplexed imaging and spatial analysis. *Nat. Protoc.* 14: 3084–3115.

6. Emamaullee, J. A., S. Toso, N. Merani, A. A. Bigam, N. Kneteman, et al. 2022. Spatial profiling of immune and inflammatory responses in human liver transplant rejection using imaging mass cytometry. *Front. Immunol.* 13: 843105.

7. Greenwald, N. F., G. Miller, E. Moen, A. Kong, A. Kagel, et al. 2022. Whole-cell segmentation of tissue images with human-level performance using large-scale data annotation and deep learning. *Nat. Biotechnol.* 40: 555–565.

8. Bendall, S. C., E. F. Simonds, P. Qiu, E. A. Amir, P. O. Krutzik, et al. 2011. Single-cell mass cytometry of differential immune and drug responses across a human hematopoietic continuum. *Science* 332: 687–696.

9. Jolliffe, I. T., and J. Cadima. 2016. Principal component analysis: a review and recent developments. *Philos. Trans. R. Soc. A Math. Phys. Eng. Sci.* 374: 20150202.

10. MacQueen, J. 1967. Some methods for classification and analysis of multivariate observations. In *Proceedings of the Fifth Berkeley Symposium on Mathematical Statistics and Probability*. University of California Press, Berkeley, CA. 281–297.

11. McInnes, L., J. Healy, and J. Melville. 2018. UMAP: Uniform Manifold Approximation and Projection for dimension reduction. *arXiv* 1802.03426.

12. van der Maaten, L., and G. Hinton. 2008. Visualizing data using t-SNE. *J. Mach. Learn. Res.* 9: 2579–2605.

13. Ramachandran, P., A. Dobie, J. R. Wilson-Kanamori, E. Dora, B. E. Henderson, et al. 2019. Resolving the fibrotic niche of human liver cirrhosis at single-cell level. *Nature* 575: 512–518.